Design Parameter Optimization for Perpendicular Magnetic Recording Systems

Panu Chaichanavong[1,2], H. Neal Bertram[1], *Fellow, IEEE*, and Paul H. Siegel[1], *Fellow, IEEE*

[1]Center for Magnetic Recording Research, University of California at San Diego, La Jolla, CA 92093 USA
[2]Marvell Semiconductor, Santa Clara, CA 95054 USA

In a perpendicular magnetic recording system, advanced read/write transducers, magnetic media, and signal processing techniques are combined to achieve the highest possible storage density, subject to severe constraints on reliability. This paper proposes a quasi-analytic methodology for exploring the complex design tradeoffs among these system components. We use a simple channel model, characterized by three parameters: isolated voltage pulse width, transition jitter noise variance, and additive electronic/replay head noise power. The system incorporates generalized partial-response equalization and maximum-likelihood detection, along with a Reed–Solomon error-correcting code characterized by its code rate. We calculate a family of "design curves" from which we can determine, for a given set of channel parameters, the maximum user density that can be achieved with a specified codeword error rate, along with the corresponding code rate. The design curves can also be used to determine the acceptable range of channel parameters consistent with a target user density and codeword error rate.

Index Terms—**Additive noise, jitter noise, parameter optimization, perpendicular recording, Reed–Solomon code, Viterbi detector.**

I. Introduction

THE increased storage density achieved by advanced magnetic recording technology relies on the improvement of several system components, including heads, media, and signal processing. The relationship among these components is complex, and the overall system optimization is a difficult engineering challenge.

This paper introduces a simulation-based methodology for the joint optimization of head, media, and signal processing parameters in a perpendicular recording system. We consider a simple channel model characterized by three parameters: the isolated pulse response width, transition jitter noise, and additive electronic/replay head noise power. The detection and coding scheme incorporates an optimized generalized partial-response (GPR) equalizer, maximum-likelihood detector, and Reed–Solomon error-correcting code.

We calculate a family of "design curves" from which we can determine, for a given set of channel parameters, the maximum user density that can be achieved while satisfying a specified sector error rate criterion. Conversely, given a target user density and sector error rate, we can determine from the design curves an acceptable range of design parameters. As a by-product, the calculation generates the corresponding equalizer target, minimum mean-squared-error (MMSE) equalizer, and Reed–Solomon code rate. It is to be emphasized that the maximum physically achievable density is ultimately constrained by limits on the grain size and thermal stability of the medium [1], [2].

A number of authors have considered recording system optimization. Ryan [3] studied the error-control design tradeoff for a PR4-equalized Lorentzian channel in a system employing turbo-like codes. In [4], Ryan *et al.* computed optimal code rates for the Lorentzian channel for two classes of codes: Shannon codes (i.e., capacity-achieving codes) and low-density parity-check (LDPC) codes. They also determined the bit-aspect ratio that maximizes areal information density by computing the achievable information rate of a data-dependent autoregressive noise model.

Optimal code rates for interleaved Reed–Solomon codes and a modulation code were presented by Cideciyan *et al.* [5]. Wood [6] explored the possibility of recording at an areal density of one terabit per square inch and predicted bit error rates for various bit spacings. He also calculated the required error correcting capabilities of Reed–Solomon codes. A similar study focusing on off-track capability was presented by Jin *et al.* [7]. A variety of other signal and noise models have been used to estimate the bit error rate (as opposed to the sector error rate) of recording systems [8]–[11].

What distinguishes the system optimization methodology introduced in this paper from previous approaches is the quasi-analytic technique used to determine design curves that more clearly reveal the design tradeoffs among the primary perpendicular recording channel parameters, the channel bit spacing, and the error-correcting code rate.

This paper is organized as follows. Section II describes our channel model for perpendicular recording and identifies the key system parameters that we consider in our analysis. In Section III, we introduce the concept of design curves and show how the curves can be used to address the system optimization problem. In Section IV, we describe a useful normalization of the design curves and present a quasi-analytic methodology for computing the normalized curves. Then, in Section V, we demonstrate by means of a simple example how to use the design curves to find an optimal system operating point. Section VI considers a slightly different design problem, in which the code rate is fixed, and we wish to determine the range of acceptable recording channel parameters subject to the rate constraint. Section VII introduces alternative design curves corresponding to a

Digital Object Identifier 10.1109/TMAG.2006.880080

different fixed channel parameter. Finally, in Section VIII, we describe possible directions for extending this system design methodology and its applications.

II. Channel Model

In our channel model, we consider three primary recording characteristics: the isolated voltage pulse width, the noise due to the magnetic medium, and electronic noise.

The replay voltage pulse width, denoted T_{50}, is the width at half of the maximum amplitude of the readback signal corresponding to an isolated magnetic transition. It reflects the extent of intersymbol interference (ISI) and plays a role in the design of the channel equalizer [12].

The magnetic medium noise is the dominant noise source in current magnetic recording devices. It is nonstationary and arises from magnetic properties of the recorded transitions. The dominant component of the medium noise arises from the randomness of the transition zero crossings and is referred to as "jitter noise." This noise has a spectral content similar to that of the replay signal, and it is characterized by the jitter noise variance, denoted σ_J [13]–[15]. There is also a component of stationary, uniform "dc noise" caused by the magnetic medium, but this is considered very small in perpendicular recording channels.

The electronic noise is generated by the replay transducer and the readback circuitry. This stationary noise source is modeled as bandwidth-limited, additive white Gaussian noise, and we characterize it by a signal-to-noise ratio, denoted $\mathrm{SNR_{WG}}$, which is the ratio of the peak isolated pulse voltage power to the variance of the noise. A small amount of stationary medium noise, not included in the jitter noise, can also be incorporated into the $\mathrm{SNR_{WG}}$ term.

Using these channel model parameters, we now derive the discrete-time model used in the calculation of the design curves. Let $y_k \in \{-1, +1\}$ be the recorded data. As in [12], we assume that the transition response is given by

$$s(x) = V_{\max}\mathrm{erf}\left(\frac{0.954x}{T_{50}}\right). \tag{1}$$

Define $h(x) = (s(x) - s(x - B))/2$, where B is the channel bit spacing. This function h is sometimes called the dipulse response in longitudinal recording. The noiseless signal is given by

$$V_{\mathrm{sig}}(x) = \sum_k y_k h(x - kB). \tag{2}$$

The noise comprises both the transition jitter noise and the additive white Gaussian electronic noise. The jitter noise is given by

$$V_n(x) = \sum_k \alpha_k \left(\frac{y_k - y_{k-1}}{2}\right) s'(x - kB) \tag{3}$$

where α_k are independent Gaussian random variables with mean zero and variance σ_J^2 and $s'(x)$ is the derivative of $s(x)$ (see [14]–[16]). After low-pass filtering and sampling the noisy signal with sampling interval B, we obtain the discrete-time received signal

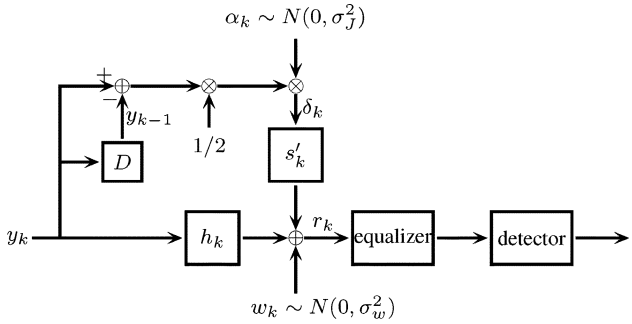

Fig. 1. Block diagram of discrete-time channel model.

$$r_k = V_{\mathrm{sig}}(kB) + V_n(kB) + w_k \tag{4}$$

where the noise samples w_k are independent Gaussian random variables with mean zero and variance σ_w^2. The signal-to-additive-noise ratio, denoted by $\mathrm{SNR_{WG}}$, is defined as

$$\mathrm{SNR_{WG}} = 10\log_{10}\left(\frac{V_{\max}^2}{\sigma_w^2}\right). \tag{5}$$

The sampled signal is passed through a finite-impulse-response equalizer and then a Viterbi detector. We used the minimum mean-squared error criterion to optimize the equalizer and target response [17]. The Appendix has some more detail on the equalizer design. This discrete-time channel model is illustrated in Fig. 1. The notations h_k and s'_k denote $h(kB)$ and $s'(kB)$, respectively.

It is important to note that, for a specified $\mathrm{SNR_{WG}}$, the discrete-time system model depends only on the normalized channel parameters T_{50}/B and σ_J/B. This fact will play a role in the computation of the design curve. The $\mathrm{SNR_{WG}}$ depends on the bandwidth and thus can depend on the bit spacing B. For a one-sided noise power spectral density N_0 (in volts squared per hertz) and a head-medium velocity v, the electronic noise variance can be written as $\sigma_w^2 = N_0 v/2B$. We discuss the consequences of more generalized scaling in the course of this paper.

III. Description of the Design Curve

The description of the channel in the previous section involved the signal parameters T_{50} and $V_{\max}$, noise parameters σ_J^2 and $\mathrm{SNR_{WG}}$, and a channel bit spacing B.

A natural question regarding the design parameter optimization is the following: Given the three channel characteristics T_{50}, σ_J^2, and $\mathrm{SNR_{WG}}$, what is the maximum achievable user density for which the sector error rate remains below a certain threshold? The design curves that we now describe provide an answer to this question. The calculation of the design curves also yields the MMSE equalizer, bit spacing B, and Reed–Solomon code rate R corresponding to the maximum density.

Define the user bit spacing $B_{\mathrm{user}} = B/R$. For fixed B_{user} and $\mathrm{SNR_{WG}}$, the design curve separates the T_{50} and σ_J plane into acceptable and unacceptable regions. The acceptable region corresponds to those pairs of T_{50} and σ_J for which there exists a Reed–Solomon code that gives a sufficiently low sector error

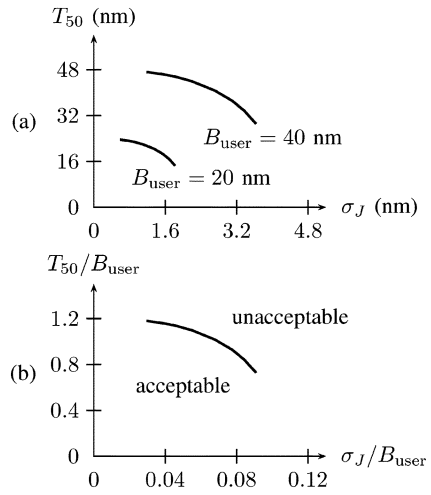

Fig. 2. (a) Design curve scales linearly with B_{user} in the radial direction. (b) Normalized design curve.

rate. The pairs in the unacceptable region are those for which the target error rate cannot be achieved.

Fig. 2(a) shows the design curves for $\text{SNR}_{\text{WG}} = 20$ dB, sector error rate threshold of 10^{-12}, and two values of user bit spacing $B_{\text{user}} = 20, 40$ nm. For each curve, the acceptable region is below the curve and the unacceptable region is above.

The design curve itself can be interpreted as pairs of T_{50} and σ_J values for which the corresponding B_{user} is the maximum achievable density. However, for a system with three length parameters: T_{50}, σ_J, and B_{user}, scaling will occur so that, as illustrated in Fig. 2(b), only one scaled curve of T_{50}/B_{user} versus σ_J/B_{user} need be plotted. This normalized curve gives design curves for any value of B_{user}.

IV. Computation of the Design Curve

To compute the normalized curve, we assume that the code employed is the Reed–Solomon code over $\text{GF}(2^{10})$ with input length of 4100 bits. Next, we set the target sector error rate to 10^{-12}, and fix a value of SNR_{WG}. As mentioned earlier, the discrete-time channel model depends only on T_{50}/B and σ_J/B. With these channel parameters fixed, we compute an equalizer and a target response that optimize the mean-squared error criterion. The equalizer is assumed to have 14 taps and the target transition response length is assumed to be 3. Then we simulate the channel and collect the error statistics at the output of the channel Viterbi detector. Based on the statistics, we can use properties of Reed–Solomon codes to calculate the highest code rate R that achieves the sector error rate. This determines the highest user density achievable with these parameters. This quasi-analytic method used to estimate sector error rates is referred to as the block multinomial method [18].

To determine a point on the normalized design curve for the specified SNR_{WG}, we carry out this calculation for a range of T_{50}/B and σ_J/B values that lie along a line of fixed slope $\rho = T_{50}/\sigma_J$. We then find the maximum user density achieved by the parameters along this line, as well as the corresponding code rate R^*. The normalized design curve is obtained by varying the slope ρ.

The computation procedure is illustrated in Fig. 3. We fix $\text{SNR}_{\text{WG}} = 20$ dB and the ratio $\rho = 20$. We vary σ_J/B from

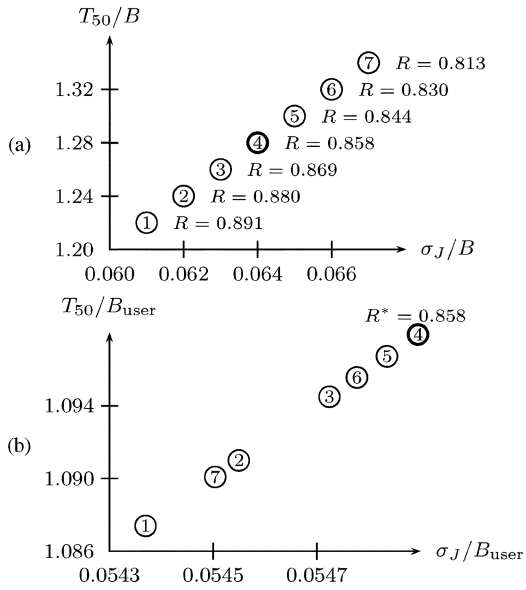

Fig. 3. Computation of a point on the design curve. (a) Range of T_{50}/B and σ_J/B that are simulated, along with the highest code rates achieving the desired error rate. (b) T_{50}/B_{user} and σ_J/B_{user} computed from the code rates in (a).

0.061 to 0.067, and so T_{50}/B is varied from 1.22 to 1.34. We denote each pair of T_{50}/B and σ_J/B by a number (from 1 to 7). For each pair, we determine the highest code rate R that achieves 10^{-12} sector error rate. This code rate is indicated in Fig. 3(a). We then compute $T_{50}/B_{\text{user}} = RT_{50}/B$ and $\sigma_J/B_{\text{user}} = R\sigma_J/B$ for all pairs as shown in Fig. 3(b). Certainly, these points lie on the acceptable side of the design curve. We see that pair 4 achieves the largest values of T_{50}/B_{user} and σ_J/B_{user}, and so these values lie at the edge of the acceptable region. In other words, pair 4 lies on the normalized design curve. The corresponding code rate $R^* = 0.858$.

The complete design curves for SNR_{WG} =14, 17, 20, 23, 26 dB are shown in Fig. 4. Table I lists the optimal code rates R^* for a range of ratios $\rho = T_{50}/\sigma_J$. Table II shows the bit error rates at the Viterbi detector output for the end points of the design curves. Fig. 4 and Table I summarize the results of all analysis in this paper including forthcoming interpretations. For example, the curves may be replotted in terms of T_{50}/B versus σ_J/B, as in Fig. 5. A more complex replotting might be to pick a value of B_{user} and evaluate $2V_{\max}^2/N_0 v$ at every point of Fig. 4. Then a plot of T_{50} versus σ_J for fixed values of $2V_{\max}^2/N_0 v$ could be made for the value of B_{user}. It is important to note that only T_{50} versus σ_J curves for a fixed SNR_{WG} have the property (as in Fig. 2) that values of parameters below a given curve will have a sector error rate of 10^{-12} or better, whereas parameters above a given curve will have worse sector error rate.

Note that the result may differ each time we compute the curve since the computation involves a Monte Carlo simulation. We find that the curve itself is not very sensitive to this, but the optimal code rate can vary, typically in the range of ± 0.02. This explains why the curves in Fig. 5 are not as smooth as those in Fig. 4.

We remark that the methodology for computing the curves can be extended to other signal and noise models, coding and detection methods, and error-rate estimation techniques.

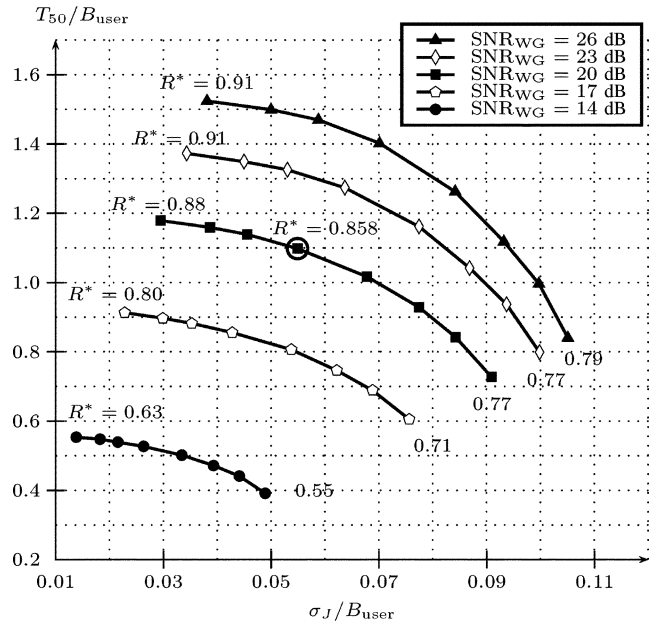

Fig. 4. Design curves for a range of values of SNR_{WG}. For scaling $\text{SNR}_{\text{WG}} = 2V_{\text{max}}^2 R^* B_{\text{user}}/N_0 v$.

TABLE I
OPTIMAL CODE RATES R^* FOR THE DESIGN CURVES IN FIG. 4

ρ	14 dB	17 dB	20 dB	23 dB	26 dB
40	0.629	0.801	0.880	0.915	0.907
30	0.637	0.801	0.865	0.887	0.903
25	0.627	0.817	0.876	0.884	0.907
20	0.627	0.807	0.858	0.872	0.887
15	0.627	0.768	0.820	0.854	0.847
12	0.605	0.785	0.801	0.847	0.847
10	0.596	0.757	0.795	0.801	0.804
8	0.551	0.712	0.774	0.768	0.785

TABLE II
BIT ERROR RATES AT THE VITERBI OUTPUT FOR BOTH END POINTS OF THE DESIGN CURVES

SNR	left end point ($\rho = 40$)	right end point ($\rho = 8$)
14 dB	2.2×10^{-2}	3.1×10^{-2}
17 dB	6.4×10^{-3}	1.4×10^{-2}
20 dB	1.8×10^{-3}	8.7×10^{-3}
23 dB	6.6×10^{-4}	9.1×10^{-3}
26 dB	8.5×10^{-4}	7.6×10^{-3}

V. APPLICATIONS OF THE DESIGN CURVE

We now present an example of how design curves can be used in practice to determine the maximum achievable density for a set of channel parameters, as well as the corresponding code rate R and channel bit spacing B.

Suppose we can manufacture a head with minimum T_{50} of 40 nm and media with minimum σ_J of 3.5 nm. Thus, the shaded area in Fig. 6 is the range of possible T_{50} and σ_J values. Assume the SNR_{WG} at the input to the equalizer is 20 dB, and the target sector error rate is 10^{-12}. From the normalized design curve in Fig. 4, we can find the value of B_{user} for which the acceptable region of the corresponding design curve just overlaps the shaded area. This occurs at a B_{user} of 44 nm, which represents the maximum density achievable with this set of components. The corresponding code rate R^* is 0.80, and the channel bit spacing at this density is $B = B_{\text{user}} R^* = 35.2$ nm.

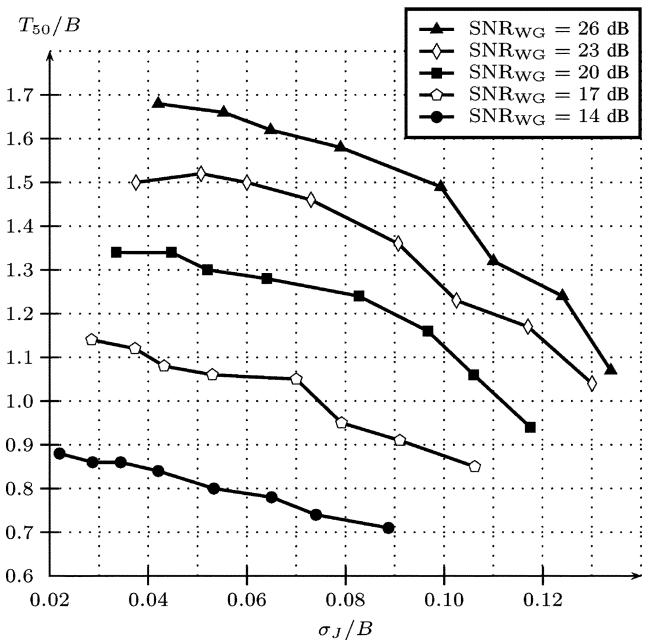

Fig. 5. Optimal values of T_{50}/B and σ_J/B for the design curves in Fig. 4. For scaling $\text{SNR}_{\text{WG}} = 2V_{\text{max}}^2 B/N_0 v$.

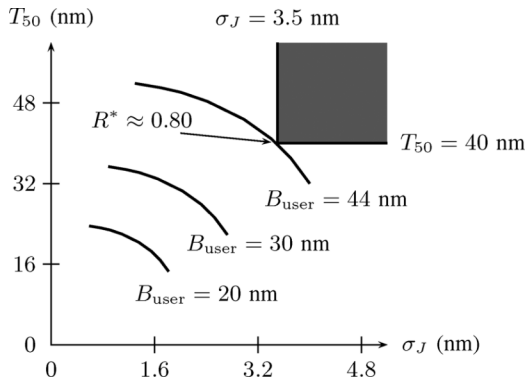

Fig. 6. Computing maximum user density using the design curve.

In the example above, SNR_{WG} was held fixed while B_{user} was varied. This would only occur if $2V_{\text{max}}^2/N_0 v$ was varied to maintain SNR_{WG}. As discussed previously, Fig. 4 may be utilized to approximately analyze the case of fixed $2V_{\text{max}}^2/N_0 v$ and varying B_{user} (see also Section VII).

Another example of the use of these design curves is to fix the areal density and explore the requirements on T_{50} and σ_J. Let us assume a channel areal density of 1 terabit per square inch. If the bit-aspect ratio (track pitch TP to channel bit spacing B) can be 4, then the channel bit spacing B is 12.7 nm (2000 kfci). Let us first assume an $\text{SNR}_{\text{WG}} = 20$ dB. Using Fig. 5, two possible design points are $T_{50}/B = 1.25, \sigma_J/B = 0.08$ and $T_{50}/B = 1, \sigma_J/B = 0.11$. The code rate varies. The jitter for these examples are $\sigma_J = 1$ and 1.4 nm, respectively. We use the jitter expression from [14] or [16] including a slight modification for noise read width. For a thermal grain diameter of 3 nm (which is optimistic) and a read width of $W_r = 0.5\text{TP} = 2B = 25.4$ nm, it might be possible to achieve such small jitter values. For this example, the required pulse widths are $T_{50} = 15.9$ and 12.7 nm, respectively. These are very

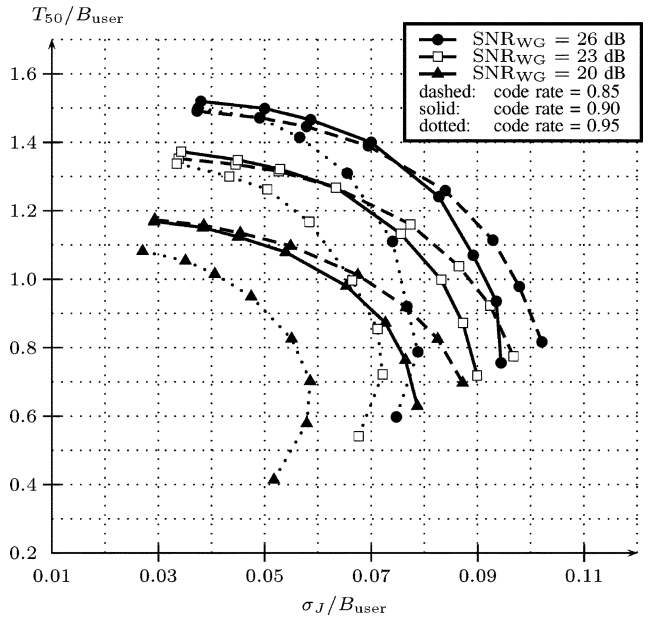

Fig. 7. Design curves for fixed code rates.

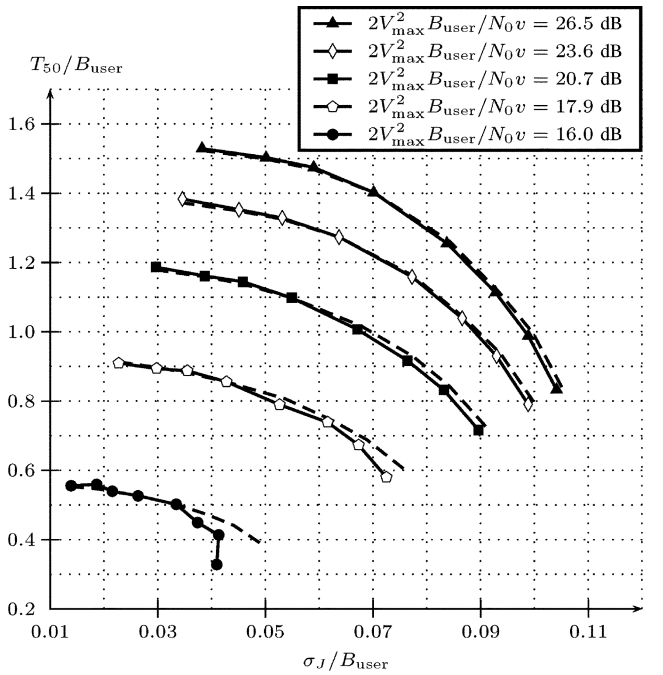

Fig. 8. Design curves with fixed $2V_{\max}^2 B_{\text{user}}/N_0 v$ obtained by interpolation. The dashed curves are the original curves in Fig. 4.

small pulse widths and would require very small head-medium spacings and replay head shield-to-shield spacings [12]. Suppose the replay head can be designed to increase SNR_{WG} to 23 dB. In that case, a possibly achievable compromise would be $T_{50}/B = 1.3, \sigma_J/B = 0.095$ or $T_{50} = 16.5$ nm, $\sigma_J = 1.2$ nm.

The design curves provide information about other system optimization issues. For example, for a specified B_{user}, the different T_{50}, σ_J pairs on the curve offer insight into tradeoffs in head and medium design. Also, the design curve calculation captures the dependence of the optimal code complexity, as reflected in the code rate, upon the extent of channel ISI, as reflected in the isolated voltage pulse width T_{50}.

VI. Design Curve For Fixed Code Rate

In practice, the channel coding scheme may have to be designed without an exact specification of the characteristics of the head and recording medium. There could be a number of possible reasons for this. First, the various system design efforts may have to proceed in parallel. Second, there may be variations in the mass-produced heads and media that preclude a single, precise component characterization. Third, different regions on the disk (such as inner and outer bands) may exhibit different signal and noise characteristics. Finally, the properties of heads and disks may change as a function of age and environment. In such a scenario, the design of the coding and signal processing techniques may have to be conservative in order to handle a wide range of component parameters.

The design curve methodology can be easily adapted for use when, as in the situations described above, the code rate may be fixed. Fig. 7 shows the normalized curves corresponding to code rates 0.85, 0.90, and 0.95, with the same target sector error rate of 10^{-12}.

VII. Design Curve for Fixed Noise Power Spectral Density

So far, we assume that a design curve corresponds to a fixed SNR_{WG}. However, $\text{SNR}_{\text{WG}} = V_{\max}^2/\sigma_w^2 = 2V_{\max}^2 B/N_0 v$. Hence, SNR_{WG} depends on B, which is not a fixed channel parameter. Thus, an alternative design curve may correspond to a fixed $2V_{\max}^2/N_0 v$ instead of SNR_{WG}. The curves can be normalized in a similar manner; they can be plotted on the T_{50}/B_{user} and σ_J/B_{user} plane with each curve corresponding to a fixed $2V_{\max}^2 B_{\text{user}}/N_0 v$.

The new design curves are more complex to compute, but they can be approximated from the original design curves by connecting the points with the same $\text{SNR}_{\text{WG}}/R^*$. Fig. 8 shows the curves obtained from the original curves by interpolation. Since the code rates R^* shown in Table I are approximately constant throughout a design curve, the new curves are close to the original ones.

VIII. Conclusion

In this paper, we introduce a quasi-analytic approach to joint optimization of design parameters in a perpendicular recording system. We adopt a linear channel model whose signal and noise characteristics are described by three parameters: the isolated voltage pulse width T_{50}, the transition jitter noise variance σ_J^2, and the signal-to-additive noise ratio SNR_{WG}, which is measured after the signal is low-pass filtered and sampled with sampling interval B. The system incorporates an optimized equalizer and maximum-likelihood sequence detector, as well as a Reed–Solomon code with code rate R.

Our results are presented in the form of design curves in the T_{50} and σ_J plane, with each curve corresponding to a fixed SNR_{WG} and user bit spacing B_{user}. Each design curve separates the plane into acceptable and unacceptable regions, with points in the acceptable region representing values of T_{50} and σ_J for which there exists a Reed–Solomon code rate that guarantees performance below a specified sector error rate. For any given SNR_{WG}, the family of curves can be normalized with respect to B_{user}, allowing them to be represented by a single curve in

the T_{50}/B_{user} and σ_J/B_{user} plane. We give a simulation-based procedure for computing the normalized design curves and illustrate their utility in several applications.

There are a number of interesting ways to extend this work. The channel model can be improved by including the effects of nonlinear transition shift, replay head nonlinearities and saturation, off-track capability, and long term thermal decay. More sophisticated signal processing and coding techniques can be considered, such as noise-predictive detection, modulation coding, parity codes with post-processing, graph-based codes with iterative decoding, and soft-decision algebraic decoding. Alternative methods for predicting sector error rates should also be evaluated. Numerical techniques for estimating the channel capacity can be used to compute design curves corresponding to the information-theoretic limits on achievable density. A more comprehensive design optimization should also account for the bit-aspect ratio, enabling the evaluation of the maximum achievable areal density. Finally, an exact computation of design curves for fixed values of $2V_{\max}^2/N_0 v$, rather than estimation from design curves with fixed SNR_{WG}, is left for future studies.

APPENDIX

For completeness, we include brief descriptions of the equalizer design and the block multinomial method here.

A. Equalizer Design

The equalizer and its target are computed using one of the techniques described by Moon and Zeng [17]. Referring to Fig. 1, y and r represent the channel input and the equalizer input. Denote the equalizer taps and its target by e and t, respectively. Then the error signal is $r*e-y*t$, where $*$ denotes the convolution. The mean-squared error can be written as

$$e^T R e + t^T Y t - 2e^T C t \tag{6}$$

where R and Y are the auto-correlation matrices for r and y, and C is the cross-correlation matrix for r and y. These matrices are functions of h, σ_J and SNR_{WG}. We optimize the mean-squared error subject to the condition that the target has unit energy: $t^T t = 1$. It was shown in [17] that this optimization reduces to an eigenvalue problem: Solve for t from $(Y-C^T R^{-1} C)t = \lambda t$ and then compute $e = R^{-1} C t$.

B. Block Multinomial Method

The block multinomial method was described in [18] as a means to estimate the error rate of a Reed–Solomon code. Let n be the length of the code in symbols. We simulate M sectors and partition the Viterbi output into non-overlapping blocks of length, say, six symbols. We count the number of blocks with e errors, $e = 0, 1, \ldots, 6$, and denote it by m_e. The probability of a block with e errors is then estimated as $p_e = 6m_e/Mn$. Assuming that each block is independent, the number of errors within one sector has the multinomial distribution. Suppose that the code can correct t errors. Then the sector error rate is

$$\sum_{s_0,\ldots,s_6} \frac{(n/6)!}{s_0! s_1! \ldots s_6!} p_0^{s_0} p_1^{s_1} \ldots p_6^{s_6} \tag{7}$$

where the summation is over the nonnegative integers s_e such that $\sum_{e=0}^{6} s_e = n/6$ and $\sum_{e=0}^{6} e s_e \geq t+1$. An efficient algorithm for evaluating the summation is given in [18]. It is based on the convolution operation.

ACKNOWLEDGMENT

This work was supported in part by the Center for Magnetic Recording Research at the University of California at San Diego, and in part by the Extremely High Density Recording (EHDR) program of the Information Storage Industry Consortium (INSIC). The authors would like to thank the anonymous referee who pointed out the design curve for fixed $2V_{\max}^2/N_0 v$, which led to Section VII.

REFERENCES

[1] Z. Jin, H. Ide, H. Zhou, P. Luo, and H. N. Bertram, "A model for bit error rate degradation during thermal decay," *IEEE Trans. Magn.*, vol. 37, no. 4, pp. 1393–1395, Jul. 2001.

[2] H. N. Bertram and M. Williams, "SNR and density limit estimates: A comparison of longitudinal and perpendicular recording," *IEEE Trans. Magn.*, vol. 36, no. 1, pp. 4–9, Jan. 2000.

[3] W. E. Ryan, "Optimal code rates for concatenated codes on a PR4-equalized magnetic recording channel," *IEEE Trans. Magn.*, vol. 36, no. 6, pp. 4044–4049, Nov. 2000.

[4] W. E. Ryan, F. Wang, R. Wood, and Y. Li, "Optimal code rates for the Lorentzian channel: Shannon codes and LDPC codes," *IEEE Trans. Magn.*, vol. 40, no. 6, pp. 3559–3565, Nov. 2004.

[5] R. D. Cideciyan, E. Eleftheriou, and S. Tomasin, "Performance analysis of magnetic recording systems," in *Proc. IEEE Int. Conf. Commun. (ICC 2001)*, vol. 9, Jun. 2001, pp. 2711–2715.

[6] R. Wood, "The feasibility of magnetic recording at 1 terabit per square inch," *IEEE Trans. Magn.*, vol. 36, no. 1, pp. 36–42, Jan. 2000.

[7] Z. Jin, H. N. Bertram, B. Wilson, and R. Wood, "Simulation of the off-track capability of a one terabit per square inch recording system," *IEEE Trans. Magn.*, vol. 38, no. 2, pp. 1429–1435, Mar. 2002.

[8] X. Che, L. C. Barbora, and H. N. Bertram, "PRML performance estimation considering medium noise down track correlations," *IEEE Trans. Magn.*, vol. 29, no. 6, pp. 4062–4064, Nov. 1993.

[9] J. Fitzpatrick, H. N. Bertram, X. Che, L. C. Barbosa, and G. H. Lin, "The relationship of medium noise to system error rate in a PRML channel," *IEEE Trans. Magn.*, vol. 30, no. 6, pp. 3990–3995, Nov. 1994.

[10] G. H. Lin, X. Xing, K. E. Johnson, and H. N. Bertram, "Texture induced noise and its impact on system performance," *IEEE Trans. Magn.*, vol. 33, no. 1, pp. 950–955, Jan. 1997.

[11] X. Xing and H. N. Bertram, "Error rate analysis of PR channels in the presence of texture noise," *IEEE Trans. Magn.*, vol. 35, no. 3, pp. 2070–2079, May 1999.

[12] B. Valcu, T. Roscamp, and H. N. Bertram, "Pulse shape, resolution and signal-to-noise ratio in perpendicular recording," *IEEE Trans. Magn.*, vol. 38, no. 1, pp. 288–294, Jan. 2002.

[13] B. Slutsky and H. N. Bertram, "Transition noise analysis of thin film magnetic recording media," *IEEE Trans. Magn.*, vol. 30, no. 5, pp. 2808–2817, Sep. 1994.

[14] J. Caroselli and J. K. Wolf, "A new model for media noise in thin film media," *Proc. SPIE*, vol. 2605, pp. 29–38, 1995.

[15] ——, "Applications of a new simulation model for media noise limited magnetic recording channels," *IEEE Trans. Magn.*, vol. 32, no. 5, pp. 3917–3919, Sep. 1996.

[16] Z. Jin, P. Luo, H. N. Bertram, K. Zhang, and G. H. Lin, "Determination of transition shape by transition mode noise analysis," *J. Appl. Phys.*, vol. 91, no. 10, pp. 8706–8708, May 2002.

[17] J. Moon and W. Zeng, "Equalization for maximum likelihood detectors," *IEEE Trans. Magn.*, vol. 31, no. 2, pp. 1083–1088, Mar. 1995.

[18] Z. A. Keirn, V. Y. Krachkovsky, E. F. Haratsch, and H. Burger, "Use of redundant bits for magnetic recording: Single-parity codes and Reed–Solomon error-correcting code," *IEEE Trans. Magn.*, vol. 40, no. 1, pp. 225–230, Jan. 2004.

Manuscript received March 13, 2006 (e-mail: psiegel@ucsd.edu).